NOTATION

C_o = average concentration of the tracer, defined as the molal flow rate of tracer divided by total flow rate of water, moles/cm^3

$C_{i,j}$ = tracer concentration in annular ring (i, j), moles/cm^3

$C_{i,n}$ = tracer concentration in annular ring i at bed depth n $(=L/d_p)$, moles/cm^3

$C_{m+1,j}$ = concentration of tracer in the wall flow, moles/cm^3

$C_{E,k}$ = experimental tracer concentration in section k of collector, moles/cm^3

$C_{T,k}$ = predicted tracer concentration in section k of collector, moles/cm^3

k = identification of section in collector, that is, k = I, II, III

LITERATURE CITED

Janz, G. J., and R. P. T. Tomkins, "Conductance Cell Calibrations: Current Practices," *J. Electrochem. Soc.*, **124**, 55C (1977).

Onda, K., H. Takeuchi, Y. Maeda, and N. Takeuchi, "Liquid Distribution in Packed Columns," *Chem. Eng. Sci.*, **28**, 1677 (1973).

Specchia, V., A. Rossini, and G. Baldi, "Distribution and Radial Spread of Liquid in Two-Phase Concurrent Flows in a Packed Bed," *Ing. Chim. Ital.*, **10**, 171 (1976).

Stanék, V., and V. Kolár, "The Radial Spread and the Number of Rivulets in a Trickle Bed," *Colln. Czech. Chem. Commun.*, 39, 2007 (1974).

Manuscript received June 17, 1977; revision received December 5, and accepted December 16, 1977.

The Design of Gas Sparged Devices for Viscous Liquid Systems

S. M. BHAVARAJU

T. W. F. RUSSELL

and

H. W. BLANCH

Department of Chemical Engineering
University of Delaware
Newark, Delaware 19711

Design procedures for gas sparged contactors for both low and high viscosity liquids were developed to predict overall k_La. Bubble size close to the orifice, for moderately high gas rates, was found to increase at a rate proportional to one third power of gas rate and one tenth power of liquid viscosity. Bubble breakup phenomenon was shown to be related to liquid turbulence in the vessel rather than gas turbulence in the orifice. Procedures were developed through a simple liquid circulation model to obtain a criterion for the onset of bubble breakup. Results indicate that intense liquid mixing and high interfacial area can be achieved in low viscosity liquids by gas sparging alone. In high viscosity fluids, bubble breakup was not observed. The liquid circulation model predicts laminar flow at these experimental conditions over the complete range of gas rates observed.

SCOPE

Simple and useful procedures for designing gas-liquid contactors for a highly viscous liquid phase are not available. Some procedures exist for low viscosity liquids, but previous investigations of gas sparging in high viscosity liquids were restricted to the study of bubble formation at low gas rates near the orifice. No studies have been reported on bubble breakup phenomena at commercial scale gas rates, in either high or low viscosity systems. The hypothesis reported in the literature, that gas turbulence in the orifice can be correlated with bubble breakup and increased interfacial area, was found to fail when liquid viscosity was increased. A design procedure to predict bubble diameters as a function of gas rate, orifice diameter, and liquid viscosity for moderately high gas rates needs to be developed which is simple enough for practical use. A mechanistic model to study the bubble breakup phenomena in the commercial scale gas rate range for both low and high viscosity liquids also needs to be formulated (based on liquid turbulence rather than gas turbulence).

CONCLUSIONS AND SIGNIFICANCE

It is important in the design and scale-up of gas-liquid contactors to be able to predict mass transfer coefficients and interfacial area per unit volume independently. Design procedures for gas-liquid contactors for both low and high viscosity liquids were developed to obtain liquid phase mass transfer coefficient k_L and interfacial area a to predict the overall k_La. Results of the liquid circulation model indicate that bubble breakup, leading to higher interfacial area, depends on the liquid turbulence in the vessel rather than gas turbulence in the orifice.

Design procedures to predict both the mass transfer coefficient k_L and the interfacial area in gas sparged tanks are presented. The procedures are valid for a wide range of liquid viscosities and gas flow rates and show for the first time the prime importance of liquid circulation and turbulence. Inclusion of liquid circulation in the model allow one to be more confident in the commercial scale design.

The design procedures show that intense liquid mixing

0001-1541-78-1142-0454-$01.55.

and high interfacial turbulence can be achieved in low viscosity systems with reasonable gas rates and orifice designs. As the viscosity of the liquid increases, the design procedures show increasing difficulty in achieving interfacial areas of the magnitude needed in most systems using gas sparging alone.

PREVIOUS WORK

Low Viscosity Liquids

An extensive literature exists on the formation of gas bubbles from orifices or nozzles submerged in liquids with viscosity of the order of 1 cp. There is good agreement among various investigators measuring the bubble sizes in the limit of very low gas flow rate. Agreement among investigators and between theory and experiments for moderately higher gas rates is rather poor.

Before we proceed, the nondimensional numbers used in the previous work and the present analysis need to be defined. Table 1 shows the various dimensionless groups which will be referred to in our discussions. The orifice Reynolds number Re_o was used by Leibson et al. (1956) and Davidson (1951), and it characterizes gas flow inside the orifice. The bubble Reynolds number Re_B was used by Van Krevelen and Hoftijzer (1950) to differentiate between laminar and turbulent chain bubbling. The modified orifice Reynolds number Re_{oL}, orifice Froude number Fr_o, and liquid Reynolds number Re_L are introduced in the present work, and their significance will be made clear in the later sections.

The region in the liquid phase in which experimental and theoretical studies have been carried out needs to be better defined. The liquid above the orifice can be divided into two regions, I and II, as shown in Figure 1. Region I is that volume of the system in which the bubble properties are determined by the bubble formation process at the orifice. This region is, in general, characterized by larger bubble size, lower holdup, and nonuniform distribution of bubbles across the cross section of the vessel in which there are multiple orifices. Region II is that volume in which bubble properties are determined by bulk liquid motions, which cause bubble breakup and coalescence. Except for the studies of Leibson et al. (1956) and the present work, most of the existing data and correlations are based on the studies in Region I. Miller (1974) based his design procedure on the fact that there is a different bubble size in each region, but his method of averaging using a geometric mean may not be suitable.

Three distinct regimes of bubble formation, based on gas flow rate, can be defined:

1. Very low gas rates. In this regime, bubbles of constant volume are formed. The bubble size is a function of orifice diameter, surface tension, and buoyancy. The bubble grows until its buoyancy force exceeds the surface tension force. A balance of buoyancy and surface tension forces yield the following relation for the bubble diameter:

$$d_{Bo} = \left[\frac{6\sigma\, d_o}{g(\rho_L - \rho_G)}\right]^{1/3} \tag{1}$$

Considerable experimental evidence for the validity of this theoretical relation was obtained by Van Krevelen and Hoftijzer (1950) and Datta et al. (1950). The limits of this regime as derived by Van Krevelen and Hoftijzer (1950) are

$$Q \leq \frac{0.31}{\mu_L}\left[\frac{\sigma^4 d_o^4}{g\,\Delta\rho}\right]^{1/3} \quad \text{for} \quad Re_B \leq 1 \tag{2}$$

and

$$Q \leq 1.66\left[\frac{\sigma^5 d_o^5}{\rho^3 g^2 \Delta\rho^2}\right]^{1/6} \quad \text{for} \quad Re_B >> 1 \tag{3}$$

Equations (2) and (3) are found to be in good agreement with the experimental data.

2. Moderately high gas rates. With further increase in gas rate, surface tension forces become negligible, and bubble size is determined by a balance of buoyancy, inertial, and viscous forces. In this regime, a mass balance results in the relation

$$Q = \frac{\pi}{6} d_B^3 f \tag{4}$$

If the frequency f remains constant, the relation between bubble size and gas rate can be obtained as follows:

$$d_B = [\text{const.}]\, Q^{1/3} \tag{5}$$

Davidson (1951) obtained the following correlation for bubble diameter using orifices ranging in diameter from 0.001 to 0.01 m:

$$d_B = 0.19\, d_o^{0.48}\, Re_o^{0.32} \tag{6}$$

TABLE 1

Nondimensional number	Definition	Critical values	Region of significance
Orifice Reynolds number	$Re_o = \frac{4Q\rho_G}{\pi d_o \mu_G}$	Laminar flow $Re_o = < 2\,000$ Turbulent flow $Re_o > 2\,000$	Gas flow inside the orifice
Modified orifice Reynolds number	$Re_{oL} = \frac{4Q\rho_L}{\pi d_o \mu_L}$		Gas flow with respect to liquid properties
Bubble Reynolds number	$Re_B = \frac{\rho_L U_B d_B}{\mu_L}$	Stokes' regime $Re_B < 1$ Taylor's regime $Re_B >> 1$	Bubble motion in liquids
Reynolds number of liquid circulation	$Re_L = \frac{\rho_L \vartheta_L d}{\mu_L}$	Laminar flow $Re_L < 2\,000$ Turbulent flow $Re_L > 2\,000$	Liquid motion above the orifice
Weber number of liquid circulation	$We_L = \frac{\rho_L \vartheta_L^2 d}{\sigma}$		Liquid flow above the orifice
Orifice Froude number	$Fr_o = \frac{Q^2}{g d_o}$		Gas flow inside the orifice

Leibson et al. (1956) measured the bubble sizes for the orifices ranging in diameter from 0.0004 to 0.0032 m and obtained the following correlation, which is in good agreement with Equation (6):

$$d_B = 0.18\, d_o^{1/2}\, Re_o^{1/3} \quad \text{for} \quad Re_o < 2\,000 \qquad (7)$$

A comparison of Equations (6) and (7) with Equation (4) suggests that frequency of bubble formation remains constant in this regime. Van Krevelen and Hoftijzer (1950) divided this regime into laminar and turbulent chain bubbling, based on the bubble Reynolds number Re_B. They derived the relation between bubble diameter and gas rate by starting with the mass balance relationship (4). If bubbles move in a continuous chain

$$f = U_B/d_B \qquad (8)$$

By substituting for bubble rise velocity U_B, from Stokes' relation or Taylor's relation, they obtained

$$d_B = 3.22\left[\frac{\mu_L}{\pi g\,\Delta\rho}\right]^{1/4} Q^{1/4} \quad \text{for} \quad Re_B < 1 \qquad (9)$$

and

$$d_B = 2.35\left[\frac{\rho_L}{\pi^2 g\,\Delta\rho}\right]^{1/5} Q^{2/5} \quad \text{for} \quad Re_B >> 1 \qquad (10)$$

Equations (9) and (10) describe a variable frequency of formation process unlike Equations (6) and (7), in which the frequency is found to be constant. In his design procedure, Miller (1974) uses Equations (9) and (10) for obtaining bubble size in region I.

Davidson and Schuler (1960*a*) derived the following equation for bubble diameter from a balance between buoyancy and inertial forces and neglecting the forces due to surface tension and viscosity:

$$d_B = 1.11\, Q^{2/5}/g^{1/5} \qquad (11)$$

This equation was found to be in good agreement with the experimental data at low gas rates ($Q < 3 \times 10^{-6}$ m^3/s). For higher gas rates, they have derived an implicit equation which accounts for the residual volume that forms the succeeding bubble. This relation was found to deviate considerably from the experimental data at higher gas rates. Kumar and Kuloor (1970) developed a two-stage model with an expansion stage and a detachment stage. They found better agreement of their model with the experimental data of Davidson and Schuler (1960*a*).

3. Very high gas rates. This regime follows the constant frequency regime, with increasing gas rates. At high gas rates, observations in region I indicate that bubble size continues to increase near the orifice with the formation of an apparent gas jet. The jet grows in size with the entrainment of surrounding liquid. Abramovich (1963) analyzed an air-water jet and derived a relation between jet diameter and distance from the orifice. In region II, bubble size is always found to decrease owing to breakup of bigger bubbles found in region I. Ultimately, at very high gas rates, bubble size in region II is found to remain constant owing to an equilibrium which is established between the breakup and coalescence processes. Leibson et al. (1956) described this regime as one where the gas rate is sufficiently high for the onset of bubble breakup, which they found to correspond to $Re_o > 2\,000$. This criterion assumes that bubble breakup is due to the gas turbulence in the orifice. For $Re_o > 10\,000$, they found the mean bubble diameter to be weakly dependent on gas rate and given by

$$d_{BE} = 0.71 \times 10^{-2} \times Re^{-0.05} \qquad (12)$$

It should be noted that the laminar, ($Re_o < 2\,000$) and turbulent ($Re_o > 2\,000$) regimes of Leibson et al. (1956) are based on laminar and turbulent flows of gas inside the orifice, and that the bubble breakup criteria for region II based on gas turbulence in the orifice were developed from a study of low viscosity liquids. It will be shown later that bubble breakup in high viscosity liquids is not related to gas turbulence in the orifice. It will also be shown that, in general, for both high and low viscosity liquids, bubble breakup is related to liquid turbulence in the vessel rather than gas turbulence in the orifice.

High Viscosity Liquids

All the previous studies with high viscosity liquids were in region I. Despite significant theoretical and experimental studies on gas bubbling in low viscosity liquids, there is very little information available for predicting bubble size in high viscosity liquids, and no work is reported on bubble breakup phenomena. Davidson and Schuler (1960*b*) studied bubble formation in liquids of high viscosity (0.5 to 1.04 N·s/m^2) in region I and found good agreement between their theory and experiments over a range of gas rates 0 to 5×10^{-5} m^3/s. For small gas rates, they obtained the following theoretical expression, from a balance between buoyancy and viscous forces:

$$d_B = \left(\frac{6}{\pi}\right)^{1/3}\left(\frac{4\pi}{3}\right)^{1/12}\left[\frac{15\,\mu_L\,Q}{2\,\rho_L\,g}\right]^{1/4} \qquad (13)$$

This relation was tested for an orifice diameter of 6.68×10^{-4} m, liquid viscosity ranging from 0.5 to 1.05 N·s/m^2, and gas rate ranging from 0 to 2.5×10^{-6} m^3/s. For higher flow rates, they did not obtain an explicit relationship but model predictions indicate much weaker dependency on the viscosity. Ramaknishnan et al. (1969) also studied the effect of viscosity on bubble formation both theoretically and experimentally, finding good agreement over a range of gas rates 0 to 6×10^{-5} m^3/s, orifice diameters 0.0037 to 0.007 m, and viscosity 0.04 to 0.5 Ns/m^2. But, as before, explicit relations between bubble diameters and viscosity were not obtained. Kumar and Kuloor (1970) reviewed various bubble formation studies and discussed the effects of viscosity in light of the above-mentioned studies. Thus, experimental and theoretical studies in high viscosity liquids were restricted to low and moderately high gas rates. Information on bubble behavior at very high gas rates is not available. The theoretical relations were implicit and very difficult to use.

EXPERIMENTAL ANALYSIS

Description of Experiments

A schematic flow diagram of experimental equipment is shown in Figure 2. Air was supplied from a compressed air cylinder (A), and its pressure is reduced to 60 lb/in.^{2} gauge by a pressure regulating valve (B). A long section of polyethylene tubing was used to connect the gas supply to the vertical nozzle (D), via a control valve (C). The liquid was contained in a transparent Plexiglas column of height 1.00 m and side 0.15 m. Air leaving the column was metered using a wet test meter (F). Liquids used in the experiments were water and aqueous solutions of carbopol. The rheological parameters of carbopol based on pseudoplastic power law model are shown in Table 2. The density and surface tension of all the liquids used were 1 000 Kg/m^3 and 72.0×10^{-3} N/m, respectively. The diameters of nozzles used were 0.0008, 0.0011, and 0.002 m. Bubble sizes were measured photographically. To obtain bubble sizes in regions I and II, photographs were taken at two locations in the column within 0.1 m from the nozzle and at about 0.8 m from the nozzle.

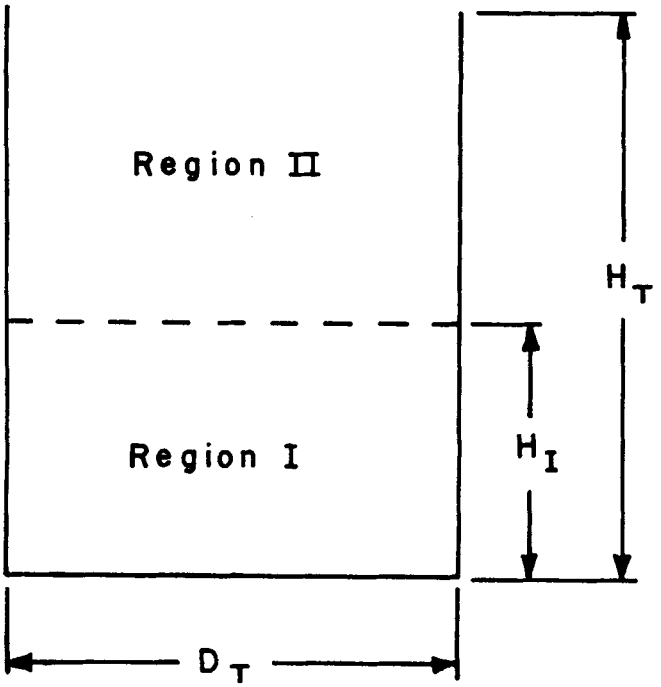

Fig. 1. Regions I and II.

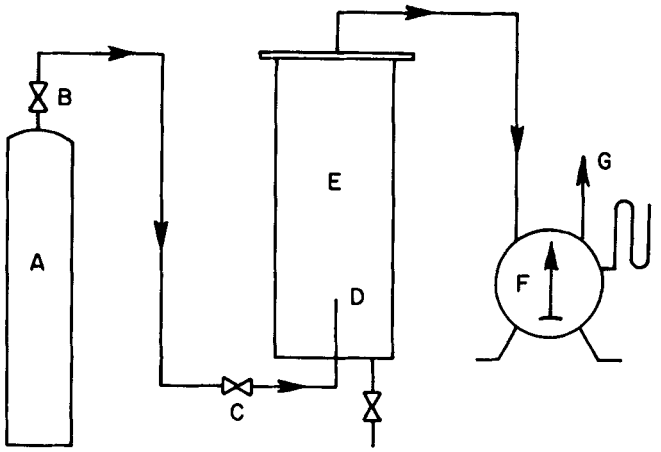

Fig. 2. Experimental setup.

TABLE 2

Weight % of Carbopol	n	K	μ_{ap}* (poise)
0.10	0.83	0.48	0.3 ~ 0.34
0.15	0.59	6.60	2 ~ 3
0.20	0.38	25.00	6 ~ 7

* $\mu_{ap} = K\left[\frac{U_B}{d_B}\right]^{n-1}[1 + X_D]$

Results. The measured bubble sizes as a function of gas rate and viscosity for region I are shown in Figure 3. These data were obtained by using orifices of diameters as given above over a range of gas rates from 10^{-6} to 2×10^{-4} m³/s. Bubble diameter was found to increase at a rate proportional to one third power of gas rate, one tenth power of apparent viscosity and found to be essentially independent of orifice diameter. Figure 4 shows the bubble diameter obtained in region II as a function of gas rate and weight percent of carbopol. It can be seen that in the case of water and 0.1% carbopol, the bubble diameter increases at a rate proportional to one third power of gas rate and then decreases with further increase in gas rate. In the case of 0.15 and 0.2% carbopol solutions, bubble size is not found to decrease even when the gas rate is increased to 2×10^{-4} m³/s ($Re_o = 1.8 \times 10^4$). It can be seen that onset of bubble breakup does not occur in high viscosity liquids even for $Re_o >> 2\,000$. The data presented in this section and the work of previous investigators will be analyzed in the following sections for both regions I and II, as defined before in Figure 1.

ANALYSIS OF BUBBLE FORMATION PROCESS

Region I

Very low gas rates. In this regime, the bubble diameter can be calculated by using Equation (1). The transition gas flow rate below which this relation is valid can be obtained as follows. Since a bubble of constant volume rises at fixed velocity, the distance between the successive bubbles is inversely proportional to the frequency of formation. Thus, distance of separation can not be less than the diameter of the bubbles formed. Hence, above a certain transition gas flow rate, the total amount of gas can not be transported by bubbles whose diameter is given by Equation (1). Above this transition gas rate (Figure 5), the bubble size increases. This transition gas rate Q_T is given

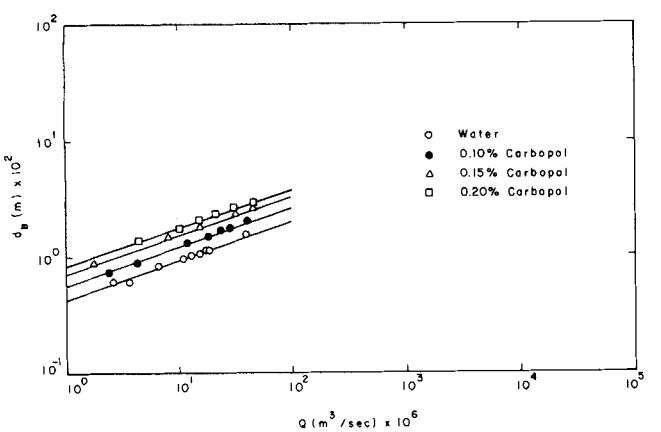

Fig. 3. Bubble diameter vs. gas rate in region I.

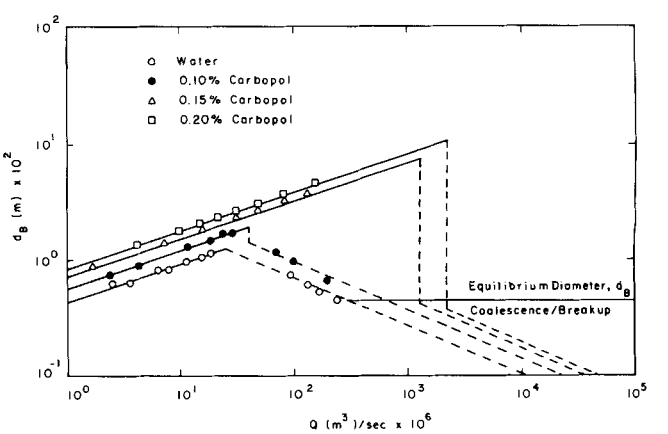

Fig. 4. Bubble diameter vs. gas rate in region II.

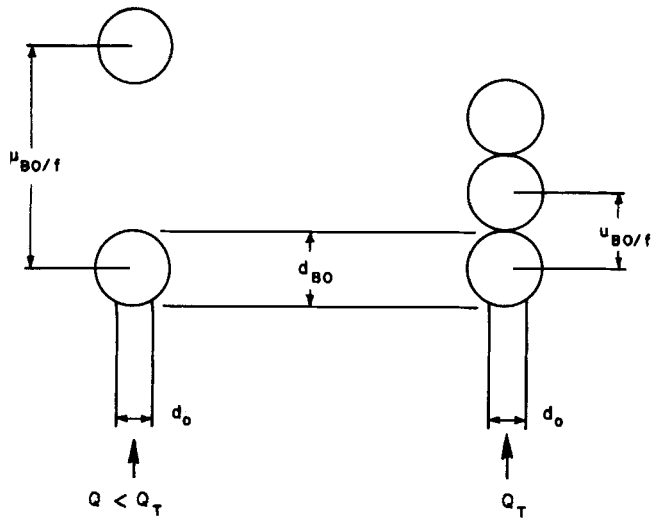

Fig. 5. Transition from constant volume to constant frequency bubble formation.

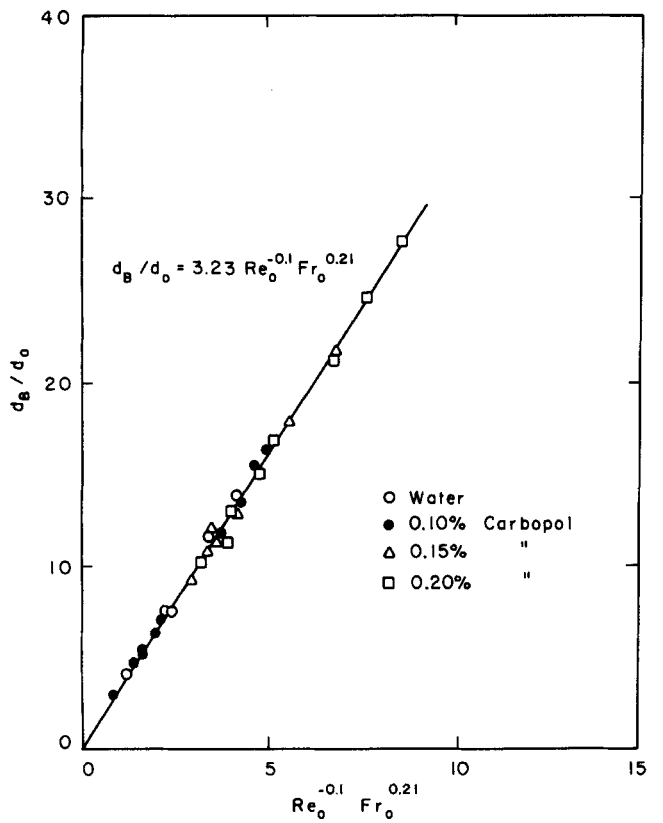

Fig. 7. Bubble diameter as a function of modified orifice Reynolds number and Froude number.

by

$$Q_T = \frac{\pi}{6} d_{Bo}^2 f_T \tag{14}$$

where

$$f_T = U_{Bo}/d_{Bo} \tag{15}$$

The rise velocity U_{Bo} of the bubble whose diameter is d_{Bo} is given by Stokes' relation

$$U_{Bo} = \left[\frac{g\rho_L}{18\,\mu_L}\right] d_{Bo}^2 \quad \text{for} \quad Re_B < 1 \tag{16}$$

and Mendelson's relation

$$U_{Bo} = \left[\frac{2\sigma}{\rho_L\, d_{Bo}} + \frac{g\, d_{Bo}}{2}\right]^{0.5} \quad \text{for} \quad Re_B >> 1 \tag{17}$$

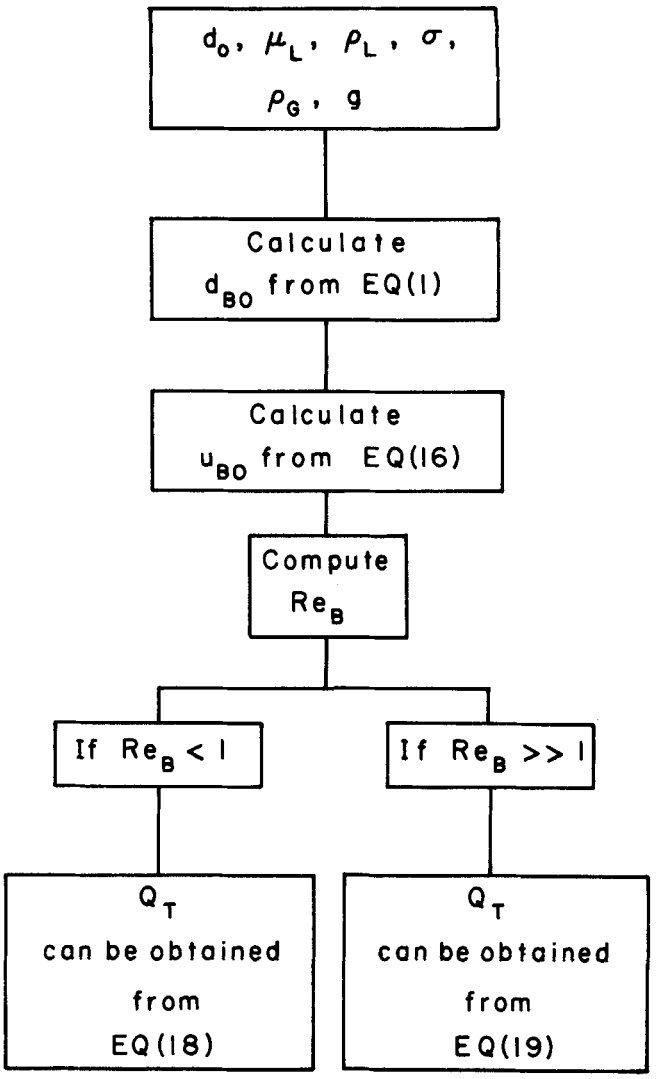

Fig. 6. Procedure for obtaining Q_T.

Substituting these for U_{Bo} and Equation (1) for d_{Bo} in Equation (14), we can obtain the transition gas rate Q_T as

$$Q_T = \frac{\pi g(\rho_L - \rho_G)}{108\,\mu_L}\left[\frac{6\sigma\, d_o}{g(\rho_L - \rho_G)}\right]^{4/3} \quad \text{for} \quad Re_B < 1 \tag{18}$$

$$Q_T = 0.38\, g^{1/2}\left[\frac{6\sigma\, d_o}{g(\rho_L - \rho_G)}\right]^{5/6} \quad \text{for} \quad Re_B >> 1 \tag{19}$$

A procedure for calculating this transition gas rate Q_T for a given gas-liquid system and orifice diameter is illustrated in Figure 6. These Equations (18) and (19) are the same as those obtained by Van Krevelen and Hoftijzer (1950), Equations (2) and (3). They derived those equations with the assumption that bubble diameter given by Equation (1) should be the same as that given by Equations (9) and (10), at the transitional gas rate Q_T.

Moderately high gas rates. For gas rates above those obtained by Equation (18) or (19), the experimental data obtained in this study (Figure 3) show that the bubble diameter increases at a rate proportional to one third power of gas rate and one tenth power of liquid viscosity. This result, along with Equation (4), suggests that the frequency of bubble formation is constant. These data are correlated, as shown in Figure 7, in terms of modified orifice Reynolds number Re_{oL} and orifice Froude number Fr_o, as follows:

$$\frac{d_B}{d_o} = 3.23\, Re_{oL}^{-0.1}\, Fr_o^{0.21} \qquad (20)$$

where

$$Re_{oL} = \frac{4\rho_L Q}{\pi d_o \mu_L} \qquad Fr_o = \frac{Q^2}{d_o^5 g}$$

Thus, bubble size in this regime can be obtained from Equation (2) as a function of gas rate and liquid viscosity. For low viscosity liquids, this relation (20) is in good agreement with Equations (7) and (6) obtained by Leibson et al. (1956) and Davidson (1951). For high viscosity liquids, explicit design equations such as Equation (20) are not available. A qualitative comparison with the implicit iterative solutions obtained by Davidson and Schuler (1960*b*) and Kumar and Kuloor (1970) support the one tenth power dependency of bubble diameter on viscosity.

Region II

Experimental data obtained in a study suggest that before the onset of bubble breakup, bubble size in region II can be safely assumed to be equal to the bubble size in region I as shown in Figures 3 and 4. But with the onset of bubble breakup, the mean bubble size in region II decreases with increase in the gas rate owing to turbulence in the liquid as suggested earlier.

Turbulent Regime. Leibson et al. (1956) described this regime as one where gas rate is sufficiently high for the onset of turbulent flow of gas in the orifice.

As shown in Figure 4, for a liquid of apparent viscosity 0.6 N·s/m², bubble breakup is absent even for $Re_o >$ 20 000 These observations suggest that bubble breakup is not related to gas turbulence in the orifice but to liquid turbulence in region II. Colored tracer studies clearly indicated that liquid circulation rates are significantly lower in high viscosity liquids as would be expected. This suggests that in high viscosity liquids, absence of bubble breakup is due to the absence of liquid turbulence, even when the gas is turbulent in the orifice. To confirm this hypothesis rather quantitatively, a simple liquid circulation model is developed and the breakup phenomena interpreted in terms of this model.

Liquid Circulation Model

Consider a gas sparged tank of diameter D and filled with liquid up to a height of H. It is known that in many such systems an overall liquid circulation develops, while the dispersed gas phase collects more or less in a concentric zone (Rietema and Ottengraf, 1970). Denevers (1968) observed strong circulation of water in an air sparged column and suggested it was caused by the density difference between those parts which are rich with dispersed phase and the parts which are poor. Towell et al. (1965) observed that rising bubbles can cause intense turbulence and mixing. They observed liquid flow downwards near the walls and upwards near the center.

Let d be the diameter of an imaginary tube separating the upflow and downflow zones as shown in Figure 8. Steady state macroscopic energy balance for the gas phase over the control volume shown in Figure 8 can be written as

$$\Delta[\tfrac{1}{2} u^2] + \Delta\overline{\Phi} + \int_{p_1}^{p_2} \frac{dp}{\rho_G} + \overline{W} + \overline{E}_U = 0 \qquad (21)$$

Neglecting the change in potential energy per unit mass $\overline{\Phi}$ and the friction loss per unit mass $\overline{E}_U$, we can express the work done by the unit mass of the gas on the liquid as

$$\overline{W} = -\int_{p_1}^{p_2} \frac{dp}{\rho_G} + \Delta[\tfrac{1}{2} U^2]$$

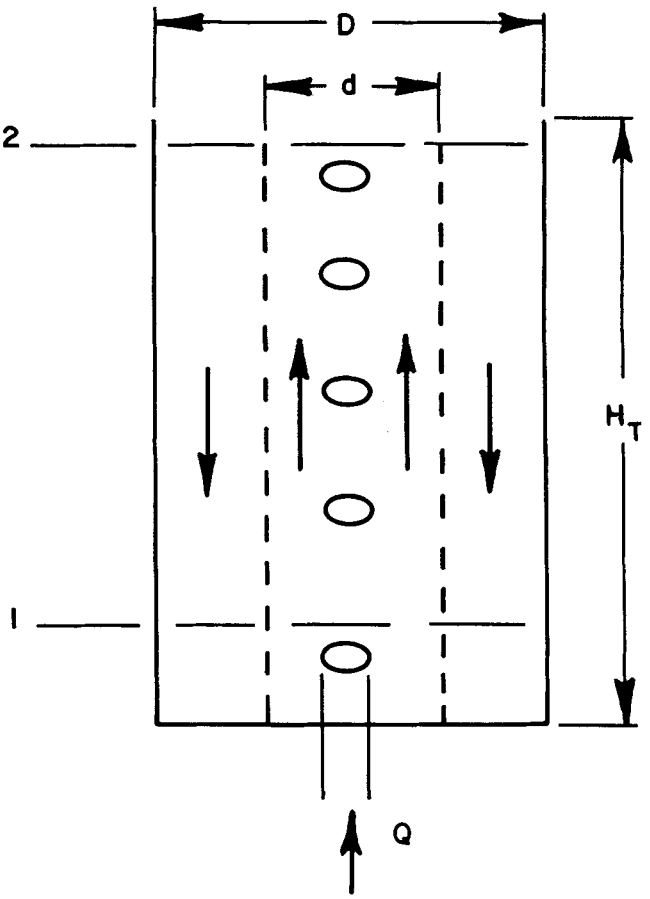

Fig. 8. Liquid circulation model.

$$= \frac{RT}{M} \ln \frac{p_1}{p_2} + \tfrac{1}{2}[U_1^2 - U_2^2] \qquad (22)$$

Neglecting the velocity U_2 and relating U_1^2 to orifice velocity U_o as suggested by Miller (1974), we obtain

$$\overline{W} = \frac{RT}{M} \ln \frac{p_1}{p_2} + \frac{\eta U_o^2}{2} \qquad (23)$$

where for air-water system $\eta \simeq 0.06$. In general, the second term is much smaller than the first term, and thus the power input can be expressed as

$$P = Q\, \rho_G \frac{RT}{M} \ln \frac{p_1}{p_2} \qquad (24)$$

Since $p_1 = p_2 + \rho_L g H$, power input can be expressed in a more convenient form

$$P = Q_M\, \rho_L g H \qquad (25)$$

where

$$Q_M = Q\, p_2/p_{LM} \quad \text{and} \quad P_{LM} = \frac{p_1 - p_2}{\ln p_1/p_2}$$

Steady state macroscopic energy balance for the liquid phase over the control volume shown in Figure 8 can be written as

$$\Delta[\tfrac{1}{2} v^2] + \Delta\overline{\Phi} + \frac{\Delta p}{\rho_L} + \overline{W} + \overline{E}_v = 0 \qquad (26)$$

Hence, the rate at which energy is lost is given by

$$\Delta\left[\frac{1}{2} v^2 \cdot \rho_L A v\right] + \Sigma \frac{1}{2} \rho_L v^2 \cdot A f v \qquad (27)$$

Thus, we obtain

$$Q_M \rho_L g H = \left\{ \frac{1}{2} \rho_L \pi d^2 v_I^3 - \frac{1}{2} \rho_L \pi (D^2 - d^2) v_A^3 \right\}$$

$$+\left\{\frac{1}{2}\rho_L \pi d H v_I^3 f_I + \frac{1}{2}\rho_L (D+d)\pi v_A^3 f_A\right\} \quad (28)$$

This can be rearranged as follows:

$$\frac{2Q_M g}{\pi d} = v_I^3 \left\{ \left[1 - \frac{1}{\left(\frac{D^2}{d^2} - 1\right)^2} \right] \frac{d}{H} + \left[1 + \frac{\left(\frac{D}{d} + 1\right)}{\left(\frac{D^2}{d^2} + 1\right)^3} \cdot \frac{f_A}{f_I} \right] f_I \right\} \quad (29)$$

Newtonian Fluid

Laminar flow. For laminar liquid flow

$$f = 16/Re_L \quad \text{where} \quad Re_L = \frac{\rho_L v d}{\mu_L}$$

1. For $f_I >> d/H$, Equation (29) gives

$$v_I = \left[\frac{Q_M g \rho_L}{8\pi \mu_L F_{L_1}}\right]^{1/2} \quad (30)$$

where

$$F_{L_1} = \left[1 + \frac{\left(\frac{D}{d} + 1\right)^2}{\left(\frac{D^2}{d^2} - 1\right)^3} \right] \quad (31)$$

2. For $f_I << d/H$, Equation (29) gives

$$v_I = \left[\frac{2Q_M g H}{\pi d^2 F_{L_2}}\right]^{1/3} \quad (32)$$

where

$$F_{L_2} = \left[1 - \frac{1}{\left(\frac{D^2}{d^2} - 1\right)^2} \right] \quad (33)$$

3. For $f_I \simeq d/H$, Equation (29) gives

$$v_I^3 \left[F_{L_2}\frac{d}{H}\right] + v_I^2 \left[F_{L_1} \cdot \frac{16\mu_L}{\rho_L d}\right] = \frac{2Q_M g}{\pi d} \quad (34)$$

v_I can then be obtained by solving the above cubic equation.

Turbulent Flow. Since $Re_L > 2\,000$, for this case, $f_I << d/H$. Hence the velocity is given by Equation (32). These velocities can be expressed in terms of Reynolds number of liquid in the inner tube as follows:
Laminar flow:

1. $f_I >> d/H$

$$Re_L = \left[\frac{Q_M g \rho_L{}^3 d^2}{8\pi \mu_L{}^3 F_{L_1}}\right]^{1/2} \quad (35)$$

2. $f_I << d/H$

$$Re_L = \left[\frac{2Q_M g H \rho_L{}^3 d}{\pi \mu_L{}^3 F_{L_2}}\right]^{1/3} \quad (36)$$

Tubulent flow:
Same as Equation (36).

Non-Newtonian Power Law Fluid

Laminar flow. For laminar flow of a power law fluid

$$f = 16/Re_{L,\,gen} \quad (37)$$

where

$$Re_{L,\,gen} = \frac{\rho_L v_I^{2-n} d^n}{k} \cdot 8\left[\frac{n}{6n+2}\right]^n \quad (38)$$

For $f_I >> d/H$, Equation (29) gives

$$v_I = \left[\frac{Q_M g \rho_L F(n)}{8\pi k d^{1-n} F_{Lp}}\right]^{\frac{1}{1+n}} \quad (39)$$

where

$$F(n) = 8\left[\frac{n}{6n+2}\right]^n \quad (40)$$

and

$$F_{Lp} = \left[1 + \frac{\left(\frac{D}{d} + 1\right)}{\left(\frac{D^2}{d^2} - 1\right)^{1+n}\left(\frac{D}{d} - 1\right)^n} \right] \quad (41)$$

For $f_I << d/H$ and for turbulent flow, the velocity is given as before by

$$v_I = \left[\frac{2Q_M g H}{\pi d^2 F_{L_2}}\right]^{1/3} \quad (42)$$

For $f_I \simeq d/H$, Equation (29) along with Equations (37) and (38) gives

$$v_I^3 \left[F_{L_2}\frac{d}{H}\right] + v_I^{1+n}\left[F_{Lp}\frac{16k}{F(n)\rho_L d^n}\right] = \frac{2Q_M g}{\pi d} \quad (43)$$

v_I can then be obtained by solving the above equation, where F_{Lp} is given by

$$F_{Lp} = 1 + \frac{\left(\frac{D}{d} + 1\right)}{\left(\frac{D^2}{d^2} - 1\right)^{1+n}\left(\frac{D}{d} - 1\right)^n} \quad (44)$$

These velocities can be expressed in terms of generalized Reynolds number as follows:
Laminar flow:
for $f_I >> d/H$

$$Re_{L,\,gen} = \left[\frac{(Q_M g)^{2-n}\rho_L{}^3 d^{4n-2} F(n)^3}{(8\pi F_{Lp})^{2-n} k^3}\right]^{\frac{1}{1+n}} \quad (45)$$

for $f_I << d/H$

$$Re_{L,\,gen} = \left[\frac{(2Q_M g H)^{2-n}[\rho_L F(n)^3]}{(\pi F_{L_2})^{2-n} k^3 d^{4-5n}}\right]^{1/3} \quad (46)$$

Turbulent flow:
Same as Equation (46). With the relations developed thus far, the Reynolds number of liquid in the inner tube can be calculated to check whether circulation is laminar or turbulent.

Since the power input is given by

$$P = Q_M \rho_L g H \quad (47)$$

and the volume of inner tube is given by

$$V_I = \frac{\pi}{4} d^2 H \quad (48)$$

the power per unit volume of inner tube is given by

$$\frac{P}{V_I} = \frac{4Q_M \rho_L g}{\pi d^2} \quad (49)$$

Now the mean bubble diameter in the inner tube can be expressed in terms of power per unit volume following Calderbank (1967)

Table 3

Q (m^3/s)	Re_L Water	0.1% carbopol	0.15% carbopol	0.2% carbopol
1×10^{-6}	1.2×10^4	353	3.5	0.25
50×10^{-6}	4.42×10^4	1 627	112.5	24.3
100×10^{-6}	5.57×10^4	2 131	208.5	54.7
150×10^{-6}	6.37×10^4	2 495	299.1	87.9
200×10^{-6}	7.02×10^4	3 747	386.4	123.1

$$d_{BM} = C_1 \frac{\sigma^{0.6}}{\left(\frac{P}{V_I}\right)^{0.4} \rho_L^{0.2}} \left[\frac{\mu_{app}}{\mu_G}\right]^{C_2} \tag{50}$$

where

$$\mu_{app} = K\left[\frac{v_I}{d}\right]^{n-1} \frac{1}{F(n)}$$

The constants C_1 and C_2 were obtained by fitting this relation with the experimental data as shown by the dashed lines in Figure 4 and were found to be $C_1 = 0.7$ and $C_2 = 0.1$, respectively:

$$d_{BM} = 0.7 \frac{\sigma^{0.6}}{\left(\frac{P}{V_I}\right)^{0.4} \rho_L^{0.2}} \left[\frac{\mu_{app}}{\mu_G}\right]^{0.1} \tag{51}$$

Thus, in this section we have developed procedures for calculating mean bubble size d_{BM} in region II. It is to be noted that in using the liquid circulation model to obtain the constants C_1 and C_2 in Equation (50), the inner tube diameter d is chosen to be equal to half the outer tube diameter D. In general for uniform distribution of sparger holes, d can be assumed to be equal to $D/2$, and D can be obtained based on the cross-sectional area per orifice as

$$D = \sqrt{\frac{4}{\pi}\left[\frac{\pi/4\, D_T^2}{N}\right]} = \frac{D_T}{\sqrt{N}} \tag{52}$$

For nonuniform distribution of sparger holes, D should be chosen based on the specific design of the sparger. For example, in the case of a ring sparger of diameter D_S, D can be obtained as

$$D = D_T - D_S \tag{53}$$

The requirement for the validity of Equations (50) and (51) is that the liquid Reynolds number should be sufficiently high for the existence of inertial subrange in the energy spectrum of turbulence. In other words, the scale of the energy containing eddies should be much larger than the scale of the energy dissipating eddies (Kolmogoroff scale). The ratio of the two scales can be expressed as

$$\frac{l}{\eta} = \frac{d\, \rho_L^{1/2}}{\mu_L^{3/4}} \left[\frac{P}{V}\right]^{1/4} \tag{53a}$$

where l is the scale of the energy containing eddies and η is the Kolmogoroff scale. In the low viscosity liquids for moderately high P/V, l/η is much greater than unity. Since for the same P/V, l/η decreases with increasing viscosity, the following criterion should be satisfied for Equations (50) and (51) to be valid:

$$\frac{l}{\eta} \geq 200 \tag{53b}$$

where the limit $l/\eta = 200$ is chosen based on the results of bubble sizes in 0.1% carbopol. For $l/\eta < 200$, even if Re_L is greater than 2 000, Equation (20) should be used to obtain the bubble diameter instead of Equation (51).

The liquid Reynolds numbers calculated using Equations (35) and (36) for water and Equations (45) and (46) for the carbopol solutions used in the present experiments are shown in Table 3. It is clear from this table that circulation was laminar for 0.15 and 0.2% carbopol solutions over the range of gas rates studied (0 to 2×10^{-4} m^3/s), whereas circulation was highly turbulent in the case of water. In the case of 0.1% carbopol, transition from laminar to turbulent circulation occurs at a gas rate of 4×10^{-5} m^3/s. Thus, the results of Table 3 along with the experimental data shown in Figure 4 substantiate the hypothesis that bubble breakup is related to the onset of liquid turbulence. The experimental observation that bubble breakup is absent for 0.15 and 0.2% carbopol solutions is consistent with the model, since circulation is laminar in both cases. The following conclusions can be drawn from this analysis:

1. For laminar liquid circulation, bubble size in region II can be assumed, for all practical purposes, to be equal to the bubble size in region I, and bubble breakup is absent.
2. For turbulent liquid circulation, bubble size in region II is determined by a balance between the dynamic forces of the liquid motion induced by gas flow and the surface tension forces. Bubble breakup is directly related to liquid turbulence rather than gas turbulence in the orifice.
3. Finally, at very high gas rates, bubble size reaches an asymptotic value of 0.0045 m which is an experimentally observed equilibrium diameter (d_{BE}) due to breakup and coalescence.

With the addition of electrolytes or surfactants, the equilibrium bubble diameter (d_{BE}) due to breakup and coalescence changes considerably. The effect of the electrolytes is mainly due to electrical repulsive forces which hinder coalescence between bubbles brought in contact by liquid motions. Marrucci and Nicodemo (1967) found that the mean bubble diameter in a sparged vessel is much smaller in the presence of electrolytes. Robinson and Wilke (1973) measured the gas-liquid interfacial area in the presence of electrolytes and found that the interfacial area per unit volume increases with increasing concentration of the electrolytes. Zlokarnik (1977) also obtained similar results with the addition of electrolytes. He further found that addition of certain organic materials such as alcohols, ketones, aldehydes, and acids also leads to similar enhancement in the interfacial area.

On the other hand, Yagi and Yoshida (1974) have found that addition of a surfactant (Tween 85) or an antifoam agent (Dow Corning antifoam agent AF emulsion) leads to a decrease in the overall k_La. Hence, in the presence of electrolytes, surfactants, etc., the equilibrium bubble diamter (d_{BE}) reported above could be much different from 0.0045 m.

PREDICTION OF k_La

From the present study and that of Miller (1974), it is clear that bubble size varies considerably from the bottom to the top of the vessel. Miller (1974) used a geometric mean of the bubble diameters in regions I and II to predict the overall k_La, and his calculated values of k_La were found to deviate considerably from the experimental values of k_La. He empirically correlated his data using the following correlation:

$$k_L^* = \frac{k_{L\,exp}}{k_{L\,calc}} = 1.21\, d_{BM}^{1.376} \tag{54}$$

Towell et al. (1965) also indicated these differences in

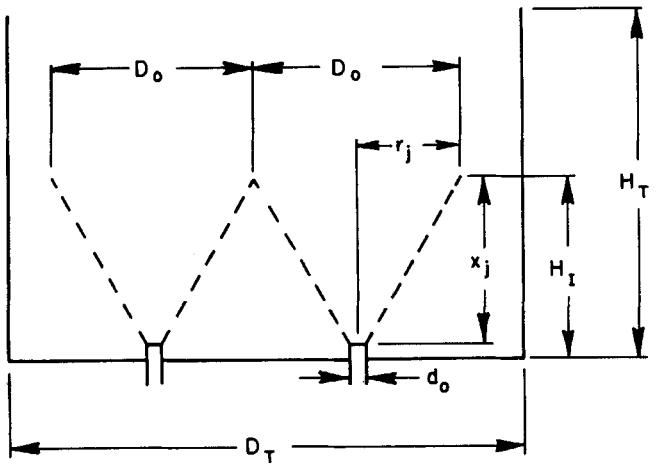

Fig. 9. Jet interaction and definition of H_I.

regions I and II. They observed that the dispersion was noticeably different near the sparger and that the differences disappear by one or two column diameters up the column. They also found that the holdup at the bottom of the tank (region I) is low because of the larger bubbles and jetting action of the gas, and further up the column (region II) the holdup reaches a constant value where larger bubbles and the jet have been eliminated by the turbulence generated in the vessel.

If the driving force in regions I and II are equal to each other and the overall driving force, then the k_La which characterizes behavior in the tank can be expressed as a weighted mean of k_La calculated in regions I and II

$$k_La = \left[\frac{H_I}{H_T}\right] k_La_I + \left[1 - \frac{H_I}{H_T}\right] k_La_{II} \qquad (55)$$

where k_La_I and k_La_{II} are values based on bubble size in regions I and II and H_I is the height of region I. Figures 3 and 4 show that bubble diameters in regions I and II are the same before the onset of breakup, and hence H_I can be assumed to be equal to H_T, the height of the tank. With the onset of bubble breakup, H_I will be less than the height of the tank, and under these conditions gas issues from the orifice in an apparent jet which disperses further up the column owing to liquid turbulence, giving rise to uniform dispersion in region II. Thus, region I can be defined as the bottom portion of the tank where gas jets are growing until they interact with the walls of the tank in the case of single orifice, or with the other jets in the case of multiple orifices. Hence, height of region I, H_I, should be dependent on tank diameter and sparger design (Figure 9).

If the apparent radius of the gas jet is defined as the distance from the axis of the jet where jet velocity is half the velocity at the jet axis, then the ratio of apparent radius of the jet (r_j) and the axial distance from the orifice can be shown to be (Abramovich, 1963)

$$\frac{x_j}{r_j} = 2.25 \qquad (56)$$

Since H_I is defined as that distance x_j for which r_j is large enough for the jet to interact with the walls or other jets, H_I depends on the sparger design. As sparger designs vary considerably, procedures for calculating H_I for certain specific sparger designs will be described below.

Case 1. For uniform distribution of sparger holes, cross-sectional area per orifice is given by

$$A_o = \frac{A_T}{N} = \frac{\pi/4\, D_T^2}{N} \qquad (57)$$

The diameter of zone of influence of a single orifice can be estimated by

$$D_o = \sqrt{\frac{4}{\pi} A_o} = \frac{D_T}{\sqrt{N}} \qquad (58)$$

Thus, height of region I, H_I, will be that distance x_j at which r_j is equal to $D_o/2$; that is

$$H_I = 2.25 \frac{D_T}{2\sqrt{N}} = 1.125 \frac{D_T}{\sqrt{N}} \qquad (59)$$

Case 2. For nonuniform distribution of sparger holes, as in the case of a ring sparger, H_I should be the distance at which the jets interact at the center of the ring; that is

$$H_I = 2.25 \frac{D_S}{2} = 1.125\, D_S \qquad (60)$$

A design procedure for predicting the mean bubble size in regions I and II and overall k_La based on the present analysis for gas sparged vessels is given below, followed by an example.

TABLE 4

I. Very low gas rates	$Q < Q_T = \frac{\pi g \Delta\rho}{108\,\mu_L}\left[\frac{6\sigma d_o}{g\Delta\rho}\right]^{4/3}$ for $Re_B < 1$ $= 0.32 g^{1/2}\left[\frac{6\sigma d_o}{g\Delta\rho}\right]^{5/6}$ for $Re_B >> 1$	$d_B = \left[\frac{6\sigma d_o}{g\Delta\rho}\right]^{1/3}$
II. Moderately high gas rates	$Q > Q_T$ and $Re_L < 2\,000$	$\frac{d_B}{d_o} = 3.23\,[Re_o]_L^{-0.1}\,[Fr_o]^{0.21}$ Equation (20)
III. Very high gas rates	$Re_L > 2\,000$	
	(i) For $d_B \mid < d_{BM}$ Equation (20)	$\frac{d_B}{d_o} = 3.23\,[Re_o]^{-0.1}\,[Fr_o]^{0.21}$ Equation (20)
	(ii) For $d_B \mid > d_{BM}$ Equation (20) $\mid > d_{BE} = 0.0045$ m Equation (51)	$d_{BM} = 0.7\left[\frac{\sigma^{0.6}}{(P/V_I)^{0.4}\,\rho_L^{0.2}}\right]\left[\frac{\mu_{ap}}{\mu_G}\right]^{0.1}$ Equation (51)
	(iii) For $d_{BM} \mid < d_{BE} = 0.0045$ m Equation (51)	$d_{BE} = 0.0045$ m

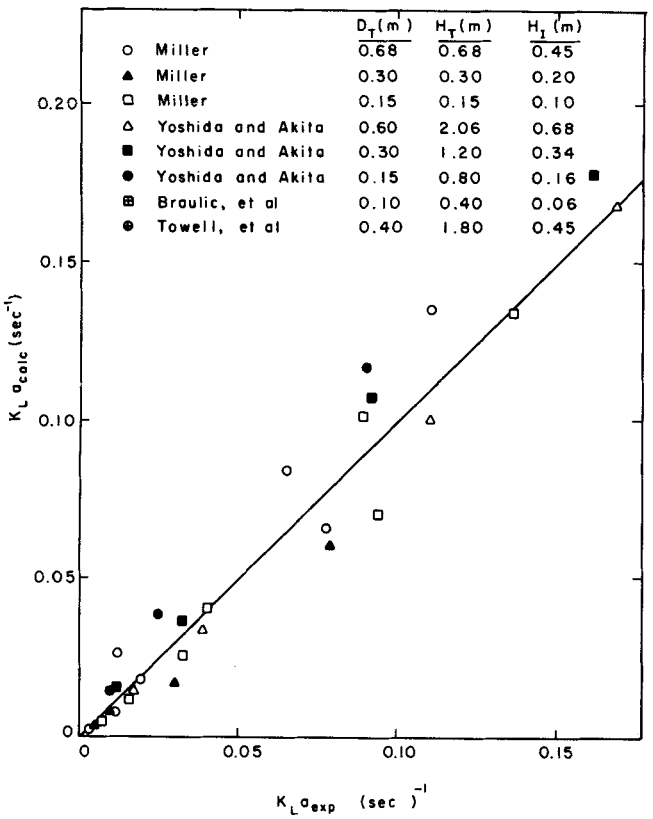

Fig. 10. Comparison of experimental and calculated values of k_La.

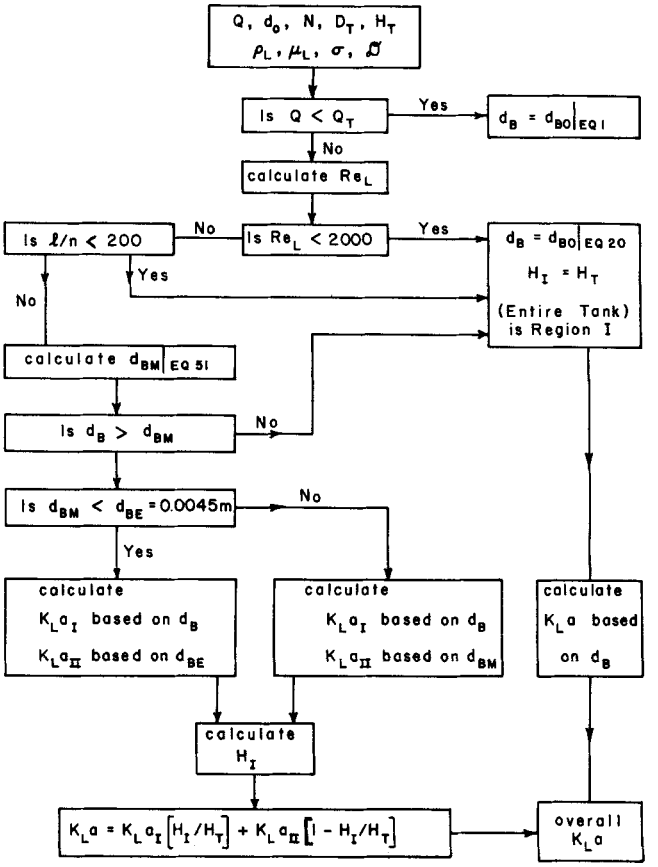

Fig. 11. Design procedure.

DESIGN PROCEDURE

Design variables:

Gas rate	Q m^3/s
Orifice diameter	d_o m
Gas and liquid densities	ρ, ρ_L Kg/m^3
Liquid viscosity	μ_L $N \cdot$ s/m^2
Surface tension	σ N/m
Diffusivity	D m^2/s
Tank diameter	D m
Sparger diameter	D_S m
Number of holes	N —
Tank height	H m

Mean Bubble Diameter

1. Calculate Q_T as shown in Figure 6. If $Q < Q_T$, bubble size can be obtained by Equation (1).
2. For $Q > Q_T$, calculate Re_L using Equation (35) or (45).
3. For $Re_L < 2\,000$, bubble size can be obtained by Equation (20), since bubble breakup is absent in this case and $H_I = H_T$.
4. For $Re_L > 2\,000$, bubble size can be obtained by either Equation (20) or (51), whichever is smaller [Equation (51) should be used only if $1/\eta \geq 200$].
5. If bubble size obtained by Equation (51) is lower than 0.0045 m, bubble size can be assumed to be constant and equal to 0.0045 m.
6. The design equations for this procedure are listed in Table 4.

Prediction of k_La

1. The liquid phase mass transfer coefficient k_L can be obtained from the relation

$$k_L = \left[\frac{4\,\mathcal{D}\,u_B}{\pi\,d_B}\right]^{1/2} \tag{61}$$

2. The gas holdup can be estimated from

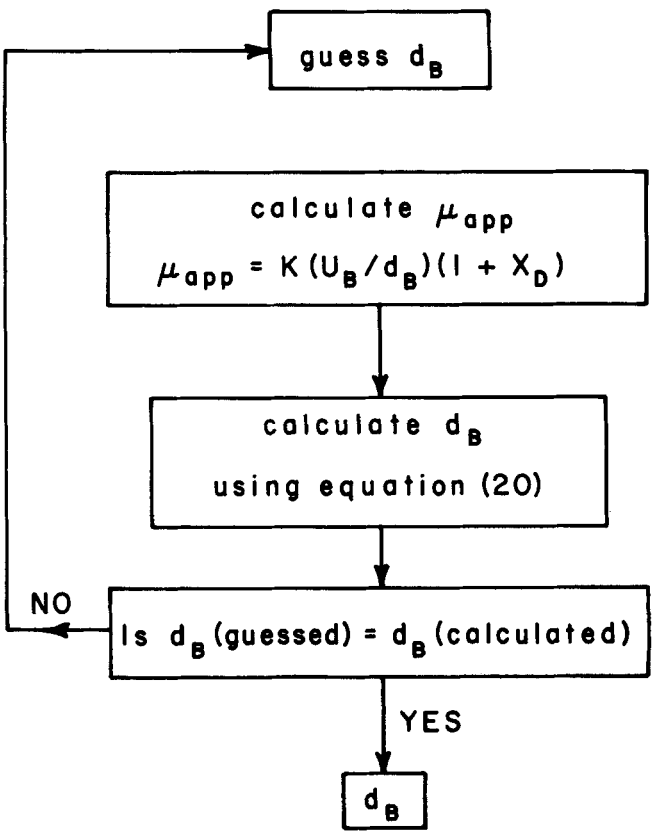

Fig. 12. Prediction of bubble size in power law fluids.

$$\phi = \frac{U_S}{U_S + U_B} \tag{62}$$

3. The terminal rise velocity of the bubbles U_B can be estimated from Stokes' relation or Mendelson's relation

as given in Equations (16) and (17).

4. The interfacial area per unit volume a can then be obtained from the relation

$$a = \frac{6\phi}{d_B} \tag{63}$$

5. Thus, k_La can be calculated from Equations (61) and (63).

6. $(k_La)_I$ for region I and $(k_La)_{II}$ for region II can be calculated using the bubble diameters obtained for regions I and II in the mean bubble diameter.

7. Calculate height of region I H_I using Equations (59) or (60); for $Re_L < 2\,000$, H_I can be set equal to H_T.

8. The overall k_La can then be calculated using Equation (55). Overall k_La calculated based on this resign procedure vs. k_La obtained experimentally for various sizes of tanks and various sparger designs, by Braulick et al. (1965), Towell et al. (1965), Yoshida and Akita (1965), and Miller (1974), is shown in Figure 10, and the agreement is good. The height of the region I for these tanks is also shown in Figure 10. It can be seen that this height (H_I) is quite significant compared to the height of the tank in these lab size tanks. The design procedure is illustrated in Figure 11.

In using Equation (20) to predict the bubble size in power law fluids, an iterative procedure needs to be followed. First, the bubble diameter should be guessed in order to calculate the apparent viscosity $[\mu_{app} = K(U_B/d_B)^{n-1}(1 + X_D)]$. The bubble diameter can then be calculated by using this apparent viscosity in Equation (20). This procedure can be repeated until the bubble diameter guessed is equal to that calculated from Equation (20). This procedure is illustrated in Figure 12.

EXAMPLE I

A 9.425 m^3 tank, 2 m in diameter and 3 m high, containing water is sparged with air at a rate of 0.071 m^3/s. It is equipped with a tree type of sparger, with forty-five holes of diameter 0.48×10^{-2} m distributed uniformly over the cross section of the tank. It is desired to predict the overall k_La.

$\mu_L = 1.0 \times 10^{-3}$ N·s/m^2
$\rho_L = 1.0 \times 10^3$ kg/m^3
$\sigma = 72.7 \times 10^{-3}$ N/m
Gas rate per orifice, $Q = 0.157 \times 10^{-2}$ m^3/s
Orifice diameter, $d_o = 0.48 \times 10^{-2}$ m
Tank diameter, $D_T = 2$ m
Tank height, $H_T = 3$ m
No. of sparger holes, $N = 45$

1. Calculation of Q_T:
   d_{Bo} [Equation (1)] $= 0.598 \times 10^{-2}$ m
   U_{Bo} [Equation (17)] $= 0.231$ m/s
   $Re_B = 1\,382$

Since $Re_B >> 1$
   Q_T [Equation (19)] $= 0.323 \times 10^{-5}$ m^3/s

2. Since $Q > Q_T$, liquid Reynolds number should be calculated.
   Outer tube diameter, D [Equation (52)] $= 0.30$ m
   Inner tube diameter, $d\,(= D/2) = 0.15$ m
   Liquid Reynolds number, Re_L [Equation (36)] $= Re_L = 1.71 \times 10^{-5}$

3. Since $Re_L >> 2\,000$, liquid circulation is turbulent.
   Bubble diameter [Equation (20)]
   $d_B = 4.88 \times 10^{-2}$ m
   Bubble diameter [Equation (51)]
   $d_{BM} = 0.384 \times 10^{-2}$ m

4. Since $d_{BM} < d_B$ and $d_{BM} < 0.45 \times 10^{-2}$ m:
   Mean diameter in region I $d_B = 4.88 \times 10^{-2}$ m
   Mean diameter in region II $d_{BE} = 0.45 \times 10^{-2}$ m

5. Now k_La can be calculated from Equations (61), (62), and (63).

   Region I
   $k_L = 0.0152 \times 10^{-2}$ m/s
   $\phi = 0.044$
   $a = 0.054 \times 10^2$ m^{-1}
   $[k_La]_I = 0.0082$ s^{-1}

   Region II
   $k_L = 0.0345 \times 10^{-2}$ m/s
   $\phi = 0.0884$
   $a = 1.178 \times 10^{-2}$ m^{-1}
   $[k_La]_{II} = 0.0406$ s^{-1}

6. Height of region I [Equation (59)] $H_I = 0.335$ m.
7. Overall k_La [Equation (55)] $= 0.0362$ s^{-1}.

It is clear from this example that intense mixing can be achieved in low viscosity liquids by gas sparging only. This example also shows that for low viscosity liquids, height of region I (H_I) in a commercial scale vessel is relatively much smaller compared to a lab size vessel.

EXAMPLE II

Rework example I for the case when liquid viscosity is 10 p.

$\mu_L = 1.0$ N·s/m^2
$\rho_L = 1.0 \times 10$ kg/m
$\sigma = 72.7 \times 10^{-3}$ N/m
Gas rate per orifice, $Q = 0.157 \times 10^{-2}$ m^3/s
Orifice diameter, $d_o = 0.48 \times 10^{-2}$ m
Tank diameter, $D_T = 2$ m
Tank height, $H_T = 3$ m
No. of sparger holes, $N = 45$

1. Calculation of Q_T:
   d_{Bo} [Equation (1)] $= 0.598 \times 10^{-2}$ m
   U_{Bo} [Equation (16)] $= 1.95 \times 10^{-2}$ m/s
   $Re_B = 0.117$

Since $Re_B < 1$
   Q_T [Equation (18)] $= 1.44 \times 10^{-6}$ m^3/s

2. Since $Q > Q_T$, liquid Reynolds number should be calculated.
   Outer diameter, D [Equation (52)] $= 0.30$ m
   Inner diameter, $d(= D/2) = 0.15$ m
   Liquid Reynolds number, Re_L [Equation (35)] $= 102$

3. Since $Re_L < 2\,000$, liquid circulation is laminar; that is, bubble breakup is absent and height of region I, H_I, is equal to height of the tank.

   Bubble diameter,
   d_B [Equation (20)] $= 9.74 \times 10^{-2}$ m

4. k_La can be calculated from Equations (61), (62), and (63).

   $d_B = 9.74 \times 10^{-2}$ m
   $k_L = 0.0128 \times 10^{-2}$ m/s
   $\phi = 0.0316$
   $k_La = 0.00025$ s^{-1}

5. Height of region II, $H_I = H_T = 3$ m.
6. Overall k_La [Equation (55)] 0.00025 s^{-1}.

This example shows that when the liquid viscosity is very high, bubble breakup is absent and the region I extends throughout the tank, giving a very low overall k_La. In the next example, a special situation will be illustrated where $Re_L > 2\,000$, but Equation (53b) is not satisfied.

EXAMPLE III

A 22.0 m^3 tank, 3.05 m in diameter and 3.05 m high, containing a liquid of viscosity 1.5 is sparged with air at rate of 0.444 m^3/s. It is equipped with a tree type of sparger with sixty holes of diameter 0.0127 m distributed uniformly over the cross section of the tank.

$\mu_L = 0.15$ n·s/m^3
$\rho_L = 1.0 \times 10^3$ Kg/m^3
$\sigma = 72.7 \times 10^{-3}$ N/m
Gas rate per orifice, $Q = 0.74 \times 10^{-2}$ m^3/s
Orifice diameter, $d_o = 1.27 \times 10^{-2}$ m
Tank diameter, $D_T = 3.05$ m
Tank height, $H_T = 3.05$ m
No. of sparger holes, $N = 60$

1. Calculation of Q_T:

d_{Bo} [Equation (1)] $= 0.83 \times 10^{-2}$ m
U_{Bo} [Equation (17)] $= 0.241$ m/s
$Re_B = 13.3$

Since $Re_B > 1$

Q_T [Equation (19)] $= 7.41 \times 10^{-6}$ m^3/s

2. Since $Q > Q_T$, liquid Reynolds number should be calculated.

Outer tube diameter, D [Equation (52)] $= 0.40$ m
Inner tube diameter, d $(= D/2) = 0.20$ m
Liquid Reynolds number, Re_L [Equation (36)] = 2 100

3. Since $Re_L > 2\,000$, liquid circulation is turbulent. But since Re_L is not very large compared to 2 000, the criterion [Equation (53*b*)] should be checked.

4. The ratio of scales of turbulence $1/\eta$ [Equation (53*a*)] = 188. Since $1/\eta < 200$, Equation (51) is not valid. Hence, as in example II, height of region I (H_I) can be assumed to be equal to the height of the tank.

5. Bubble diameter,

d_B [Equation (20)] $= 13.9 \times 10^{-2}$ m.

6. k_La can be calculated from Equations (61), (62), and (63).

$d_B = 13.9 \times 10^{-2}$ m
$k_L = 0.012 \times 10^{-2}$ m/s
$\Phi = 0.069$
$k_La = 0.00035$ s^{-1}

Thus, this example shows a situation where the criterion [Equation (53*b*)] needs to be checked.

ACKNOWLEDGMENT

This work was supported by a grant from the National Science Foundation ENG76-17004.

NOTATION

a = interfacial area per aerated liquid volume, m^{-1}
A_o = cross-sectional area per orifice, m^2
C_1 and C_2 = constants in Equation (50)
d = imaginary inner tube diameter, m
D = imaginary outer tube diameter, m
d_B = bubble diameter in region I, m
d_{BE} = equilibrium bubble diameter, m
d_{BM} = mean bubble diameter in region II, m
d_{Bo} = bubble diameter at very low gas rates, m
d_o = orifice diameter, m
D_o = diameter based on cross-sectional area per orifice, m
D_S = sparger diameter, m
D_T = tank diameter, m
$\mathcal{D}$ = diffusivity, m^2/s
f = frequency of bubble formation, s^{-1}
f_A = friction factor in the imaginary outer tube
f_I = friction factor in the imaginary inner tube
f_T = frequency of bubble formation at the onset of bubble chain formation, s^{-1}
g = acceleration due to gravity, m/s^2
H_I = height of region I, m
H_T = height of the tank, m
k_L = liquid phase mass transfer coefficient, m/s
M = molecular weight of gas
N = number of orifices
P = power input, N
P_{LM} = logmean pressure, N/m^2
P_1 = pressure at the sparger, N/m^2
P_2 = absolute pressure, N/m^2
Q = gas rate per orifice, m^3/s
Q_M = mean gas rate, m^3/s
R = gas constant, N·m/Kg·mole°K
r_j = jet radius, m
Re_o = orifice Reynolds number
T = temperature, °K
U_B = bubble rise velocity, m/s
v_A = liquid velocity in the imaginary annulus, m/s
v_I = liquid velocity in the imaginary inner tube, m/s
V_I = volume of the imaginary inner tube, m^3
X_D = correction factor for C_D for power law fluids
x_j = length of the jet from the orifice, m

Greek Letters

η = 0.06, fraction of jet energy transmitted to bulk liquid
μ_G = gas viscosity, N·S/m^2
μ_L = liquid viscosity, N·S/m^2
$\mu_{L,\,app} = K(U_B/d_B)^{n-1}(1 + X_D)$, apparent viscosity, N·S/m^2
ν = kinematic viscosity, m^2/s
ρ_G = gas density, Kg/m^3
ρ_L = liquid density, Kg/m^3
σ = surface tension, N/m
ϕ = gas holdup

LITERATURE CITED

Abramovich, G. N., *Theory of Turbulent Jets*, Mass. Inst. Technol. Cambridge, Mass. (1963).

Braulic, W. J., J. R. Fair, and B. J. Lerner, "Mass Transfer in Sparged Contactor: Part 1. Physical Mechanisms and Controlling Parameters," *AIChE J.*, 11, 73 (1965).

Calderbank, P. H., "Mass Transfer," *Mixing Theory and Practice*, Vol. 2, Chapt. 6, Academic Press, New York (1967).

Datta, R. L., D. H. Napier, and D. M. Newitt, "The Properties and Behavior of Gas Bubbles Formed at a Circular Orifice," *Trans. Inst. Chem. Engrs.*, 2, 14 (1950).

Davidson, L., "A Study of the Formation of Gas Bubbles from the Horizontal Circular Submerged Orifices," Ph.D. thesis, Columbia Univ., New York (1951).

Davidson, J. F., and B. O. G. Schuler, "Bubble Formation at an Orifice in a Viscous Liquid," *Trans. Inst. Chem. Engrs.*, 38, 144 (1960*a*).

———, "Bubble Formation at an Orifice in an Inviscid Liquid," *ibid.*, 335 (1960*b*).

Denevers, N., "Bubble Driven Fluid Circulations," *AIChE J.*, 14, 222 (1968).

Kumar, R., and N. R. Kuloor, "The Formation of Bubbles and Drops," *Adv. Chem. Eng.*, 8, (1970).

Leibson, I., E. G. Holcomb, A. G. Cacoso, and J. J. Jacmic, "Rate of Flow and Mechanism of Bubble Formation From Submerged Orifices," *AIChE J.*, 2, 296 (1956).

Marrucci, G., and L. Nicodemo, "Coalescence of Gas Bubbles in Aqueous Solutions of Inorganic Electrolytes," *Chem. Eng. Sci.*, 22, 1257 (1967).

Miller, D. N., "Scale-Up of Agitated Vessels Gas-Liquid Mass Transfer," *AIChE J.*, 20, 445 (1974).
Ramakrishnan, S., Kumar, R., Kuloor, N. R., "Studies in Bubble Formation Under Constant Flow Conditions," *Chem. Eng. Sci.*, 24, 731 (1969).
Reitema, K., and Ir. S. P. P. Ottengraf, "Laminar Liquid Circulation and Bubble Street Formation in a Gas Liquid System," *Trans. Inst. Chem. Engrs.*, 48, T54 (1970).
Robinson, C. W., and C. R. Wilke, "Oxygen Absorption in Stirred Tanks: A Correlation for Ionic Strength Effects," *Biotechnol. Bioeng.*, 15, 755 (1973).
Towell, G. D., C. P. Strand, and G. H. Ackerman, "Mixing and Mass Transfer in Large Diameter Bubble Columns," *AIChE Symposium Series No. 10* (1965).
Van Krevelen, D. W., and P. J. Hoftijzer, "Studies of Gas Bubble Formation," *Chem. Eng. Progr.*, 46, 29 (1950).
Yagi, H., and F. Yoshida, "Oxygen Absorption in Fermentors—Effects of Surfactants, Antifoaming Agents, and Sterilized Cells," *J. Ferm. Technol.*, 52, 905 (1974).
Yoshida, F., and K. Akita, "Performance of Gas Bubble Columns," *AIChE J.*, 11, 9 (1965).
Zlokarnik, M., "Influence of some Important Geometric, Material and Process Parameters on Mass Transfer in Gas-Liquid Contacting," paper presented at Engineering Foundation Conference, Henniker, N.H. (1977).

Manuscript received August 1, 1977; revision received November 21, and accepted December 7, 1977.

Cold Flow Mixing Rate Data for Pulverized Coal Reactors

VINCENT J. MEMMOTT
and
L. DOUGLAS SMOOT
Department of Chemical Engineering
Brigham Young University
Provo, Utah 84602

Mixing rates of particles and gases in confined, coaxial jets are reported for tests with conditions simulating those of pulverized coal gasification and combustion processes. Gas velocity, particle mass flux, and gas composition were measured at various radial and axial locations downstream of the primary jet exit plane. Effects of inlet velocity, density, injection angle, particle loading level, and particle size on the rates of mixing were determined. Increasing injection angle and secondary velocity significantly increased gas and particle mixing rates, while effects of other variables were much less significant. Dispersion of particles lagged that of the gas in all cases investigated.

SCOPE

Many chemical processes involve the heterogeneous mixing of gas and particulate phases. Examples of such processes are fluidized, heterogeneous, catalytic systems; pulverized coal combustors; entrained coal gasifiers; MHD power generators; and air breathing missiles. A common method of contacting the particles and the gases is to inject them from separate jets into a mixing zone. The jets may be free (exhausting into an unconfined environment) or confined by the walls of the system. Considerable effort has been expended to investigate mixing of gaseous free and confined jets. Extensive literature reviews of turbulent mixing in parallel systems have been reported by Tufts and Smoot (1971), Harsha (1971), Stowell and Smoot (1973), and Hedman and Smoot (1975). Several experimental investigations have been conducted at this laboratory to determine turbulent mixing characteristics in parallel and nonparallel coaxial jet systems. Smoot and Allred (1975) and Smoot and Fort (1976) have reported particle and gas mixing data with nonparallel injection. Smoot (1976) has summarized and correlated the experimental turbulent mixing data previously obtained at this laboratory together with data from several independent investigations.

Only limited data have been reported for experimental investigations, where the secondary-primary velocity ratio was near unity or for jets containing particles. Both are characteristic of pulverized coal combustion and gasification. Studies of Fejer et al. (1967), Beasley et al. (1970), and Durao et al. (1973) consider a primary velocity near that investigated in this study. However, these three sets of tests were performed with air containing no trace gas or particles, and only velocity data were reported. Only Beasley (1970) considers a nonparallel system with primary/secondary velocities of comparable magnitude, but without particles. No studies have been located where mixing with nonparallel injection was investigated under conditions similar to this study.

The purpose of this research was to experimentally investigate the mixing characteristics of particle laden, confined jets under conditions that would simulate industrial pulverized coal furnaces and entrained gasifiers. Radial profiles for gas composition, particle mass flux, and gas velocity were measured at various axial locations in the mixing chamber. Effects of velocity, density, injection angle, particle loading level, and particle size on the rates of particle and gas mixing were examined.

Air, argon, and silicon particles comprised the primary stream. The secondary air stream was heated with an electric circulation heater. Mixing experiments were conducted at two ratios of secondary to primary density (0.6 and 0.8) and velocity (1.3 and 2.0). Tests were also conducted at 0, 40, and 60% solids by weight in the primary jet and with three different particle size distributions. Fifty five tests were completed, of which six were conducted without particles.

Vincent J. Memmott is with Exxon Corporation, Baytown, Texas.

0001-1541-78-1140-0466-$01.05.